Two-Dimensional Aggregation of Rod-Like Particles: A Model Investigation

ARTICLE *in* THE JOURNAL OF PHYSICAL CHEMISTRY B · FEBRUARY 2002

Impact Factor: 3.3 · DOI: 10.1021/jp013209n

Two-Dimensional Aggregation of Rod-Like Particles: A Model Investigation

A. Vincze,[†] L. Demkó,[†] M. Vörös,[†] M. Zrínyi,[†] M. N. Esmail,[‡] and Z. Hórvölgyi*,[†]

Department of Physical Chemistry, Budapest University of Technology and Economics, H-1521 Budapest, Hungary, and Department of Mechanical and Industrial Engineering, Concordia University, de Maisonneuve Blvd. W., H549 Montreal, Quebec H3G 1M8, Canada

Received: August 17, 2001; In Final Form: December 11, 2001

In this work, a 2D computer model was created for the aggregation of rodlike particles, on the basis of a molecular-dynamic approach. With the help of the model, it is possible to visualize the motion of the aggregating particles, clearly and faithfully, offering the possibility of structural, kinetic, and dynamic analysis of the aggregation. The aggregation, in the model, is governed by long-range and short-range attractive particle−particle forces, two-dimensional streams, breaking forces, and the degree of particle-anisometry. The long-range forces initiate the motions of the particles and clusters and also cause restructuring in the growing aggregates, which process can be hindered by sufficiently strong short-range, attractive forces. The off-lattice computer simulation of the aggregation revealed that (i) the greater extent of restructuring resulted in the formation of denser and more compact clusters with higher fractal dimensions. Interestingly, the attractive short-range forces, through the restructuring, could also influence the driving force of aggregation. It was found that the more intensive the restructuring, the weaker the driving force is in the second stage of aggregation. (ii) An increase in the effective range of long-range forces (without restructuring) resulted in higher fractal dimensions and kinetic constants. The increase of D_f with the effective range of forces was interpreted in terms of a percolation-like aggregation. (iii) Moreover, increasing anisometry of the particles (without restructuring) also resulted in an increase of fractal dimensions, confirming that the investigated aggregations take place in a transition range between the diffusion-limited-like aggregation and percolation (gelation). Our model was implemented successfully in a real phenomenon, the aggregation of cylindrical-shaped carbon particles at water (aqueous surfactant solution)/air interfaces. The effectiveness of the computer model was proved by comparing the structural, kinetics, and mechanism-related parameters obtained for the simulations with those of the real experiments.

I. Introduction

Computer simulation is a powerful tool for getting a better insight into the aggregation phenomena.[1−8] Many present computer simulations were based on Monte Carlo methods.[9] In these models, single aggregates are grouped by a kind of selection process, and their alignment is set by an algorithm, joined, and afterward treated as one cluster. Using this method, however, only static properties (morphology) can be studied. An alternative method for the simulation of aggregations is molecular dynamics, in which the motions of the aggregating particles are governed by dynamic equations. Molecular dynamics simulations are suitable for getting information about not only the static but the dynamic and kinetic properties of the cluster formation.

The aggregation of rodlike particles has a central role in technological processes (e.g., paper making[10−12]). Numerous phenomena (e.g., lamella formation from surfactant molecules in aqueous medium[13−14] and association of polymeric and surfactant molecules[15]) can be modeled by the aggregation of rodlike particles. First, the elongated bodies as rigid ellipsoids were modeled many years ago.[16] In recent years, particle level simulations of elongated rigid or flexible bodies (fibers, rods, spheroids, plates, and their aggregates) were carried out.[17−22] The motion of these elongated bodies was perturbed by interparticle and hydrodynamic forces or friction. According to the results, the colloid interactions influence the cohesiveness of the forming network, primarily. The particle level simulations could be successfully adopted in investigating 3D sheared suspensions and sedimentations of rodlike particles. The analyses involved the examination of single fiber-dynamics, fiber flexibility, sediment, and suspension structure.

The study of solid particulate associations at liquid-fluid interfaces attracted significant attention in the last two decades. The 2D systems served as models for the investigation of general aspects of growth,[23−34] particle ordering,[35] phase transitions,[36] and surface thermodynamics.[37−40] In other cases, the examinations focused on the practical applications such as thin layer preparation by a two-dimensional sol−gel technique[41−43] and characterizations of surface properties of particles.[44−46]

The main purpose of this work is to present a computer model for the 2D aggregation of rodlike particles on the basis of molecular dynamics, which allows for the analysis of the time-dependent properties of aggregation. A novelty of this model is that a long-range and a short-range interparticle attraction is involved in it at the same time, and beyond the primary growth, a secondary process (reorganization of forming clusters) also takes place. The primary, irreversible growth is induced by the long-range attractive forces that also cause the reorganization of clusters. (It should be noted that every aggregate in the present work is considered to be a cluster without reference to their

* To whom correspondence should be addressed.
[†] Budapest University of Technology and Economics.
[‡] Concordia University.

10.1021/jp013209n CCC: $22.00
Published on Web 02/09/2002

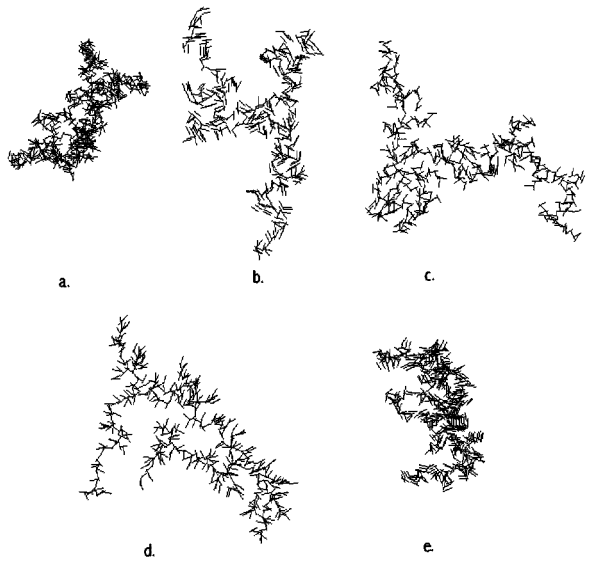

Figure 1. Visualization of the different restructuring algorithms: (a) "Rotation of clusters", (b) "Rotation of particles", (c) cluster without any kind of restructuring, (d) particle "alignment", and (e) cluster with all three restructuring algorithms. All of the aggregates were captured from a simulation with 10 000 particles, when the total number of clusters was about 200. The clusters consist of 300−350 particles.

aggregation number.) The restructuring can only occur if the short-range attractive forces are weak compared to the long-range forces. A similar model was introduced earlier for the interfacial aggregation of spherical microparticles.[47] In this work, we will provide a complex analysis of the aggregation of rodlike particles including the structure formation, the aggregation kinetics, and the mechanism. To the best of our knowledge, such a complex investigation of the aggregation of rodlike particles is unprecedented, yet.

In the following sections, we describe the main features of the computer model, show the effect of relevant parameters on the aggregation, and, finally, demonstrate the effectiveness of the model by comparing the simulation results to the results of real examinations. In the latter case, the aggregation of rodlike carbon particles has been investigated at liquid−air interfaces and analyzed using the same viewpoints described above.

II. Computer Model

In the model, the aggregation is governed by the long-range particle−particle (hereinafter p−p) forces (i), the short-range p−p forces (ii), surface streams (iii), breaking forces (iv), and the anisometry of the particles (v).

(i) The main driving force of the aggregation is the long-range attraction; thus, the use of a dynamic approach is adequate. The long-range forces affect the translational motion of the particles and clusters and also cause restructuring in the forming (and metastable) clusters. Two different restructuring algorithms were incorporated into our model: rotation of collided clusters and rotation of particles. These algorithms are not dynamic; in this model, restructuring occurs instantly instead of being continuous. The effect of different restructuring methods on the structure formation is demonstrated in Figure 1a,b. For comparison, a nonrestructuring aggregate is shown in Figure 1c. Apparently, the "rotation of clusters" algorithm has the most pronounced effect on the cluster structures. In this method, if two clusters make contact and if they are not immediately joined by an other cluster, the contact point acts as a pivot, and the two clusters rotate toward one another. This step can be repeated until a second contact forms. This algorithm can be set to allow rotations of a preset fraction of the maximum free rotational angle, resulting in a different extent of restructuring. The rotation of clusters algorithm causes global augmentation in the compactness of the clusters. The outcome of this restructuring method is shown in Figure 1a, where, the actual angle of rotation is $^1/_5$th of the maximum free rotational angle. In the second method, the independent particles that are in contact with only one cluster are rotated around the contact point toward the cluster. The particle can turn until it forms a second contact. This algorithm can also be set to rotate the particle by only a fraction of the available angle and create a more compact and smooth structure. Rotation of particles, unlike the rotation of clusters algorithm, causes only small scale, local compactness. Figure 1b shows the effect of this restructuring mechanism, if the angle of rotation is the maximum free rotational angle. An "alignment" algorithm was also developed for the moving particles. This algorithm rotates the individual particles by a preset fraction of the maximum angle. It means the cylindrical particles can be parallel or perpendicular to their velocities and can reach any position between them. The effect of "alignment" on the structure is illustrated in Figure 1d, with the angle of rotation being the maximum free rotation angle (i.e., the cylinders become perpendicular to their velocities).

(ii) Short-range forces hinder the effect of the long-range forces, reducing the extent of restructuring or preventing it altogether. Short-range attractive forces are incorporated into the model solely through the extent of restructuring mechanisms.

(iii) Our model allows the individual particles and clusters to move on their own, with the "surface streams". Streams are created by randomly positioned vortices (horizontal flow), sources, and drains, and their effects are superposed. The flows do not obey the rules of hydrodynamics; instead, they move randomly in the reaction plane.

(iv) The aggregating particles experience a drag force $\bar{F}$ that acts opposite of their velocity $\bar{v}$ and is taken into consideration as a Stokes-like force:

$$\bar{F} = c\bar{v} \tag{1}$$

where c is the decelerational variable.

(v) The anisometry (length/thickness ratio) of the rodlike particles.

III. Implementation of the Model

As a possible implementation of the general model introduced in the previous chapter, aggregation of polydisperse rodlike particles at liquid−vapor interfaces has been examined. To compare the results of computer simulations to the results of real experiments, the properties of the model were set to conform to the observed real system. The specifications of the examined real system are presented in the forthcoming subsection.

Long-Range Capillary Force. The most important aggregation-causing attractive interaction is the capillary attraction that originates from the surface tension and acts among the particles scattered on the interface. The nature of the capillary force acting between two particles floating at a liquid-vapor interface has been described.[48] For particles of low bond (or Eötvös) number this capillary force can be approximated. The definition of the bond number for a liquid-vapor interface is

$$B = \frac{gL^2}{\gamma_{A-B}}(\rho_A - \rho_B) \tag{2}$$

with g being the gravitational acceleration, L the linear size of the particle, γ_{A-B} the surface tension of the liquid−vapor

interface, and ρ_B and ρ_A the density of the liquid and the vapor. In our tests, $B \approx 1.91 \times 10^{-3}$, which proved to be a desirable value as the following eq 3 is true if $B < 10^{-1}$.

The capillary force between two spherical particles with different linear sizes (L_1 and L_2), floating at an interface, can be written as

$$F(l) = 2\pi\gamma_{A-B}L_1L_2(B_1B_2)^{5/4}S^2K_1(\lambda l) \tag{3}$$

where

$$S = \frac{2}{3}H - \frac{1}{3} - \frac{1}{2}\cos\Theta + \frac{1}{6}\cos^3\Theta \tag{4}$$

$$H = \frac{\rho_S - \rho_A}{\rho_B - \rho_A} \tag{5}$$

$$\lambda = \left[\frac{g}{\gamma_{A-B}}(\rho_B - \rho_A)\right]^{1/2} \tag{6}$$

and l is the distance between the two particles' centers of masses, Θ is the contact angle that describes the wettability, ρ_S is the density of the particles participating in the aggregation, $1/\lambda$ is an approximation of the length at which the liquid−air interface is curved around the sphere, and also of the effective range of the capillary force, and finally, $K_1(x)$ is the modified first-order Bessel function of the second kind. The behavior of the function for various x is

$$K_1(x) \approx \frac{1}{x} + O(x\ln x) \tag{7}$$

if $x \ll 1$, and

$$K_1(x) \approx \left(\frac{\pi}{2x}\right)^{1/2} e^{-x}\left(1 + O\left(\frac{1}{x}\right)\right) \tag{8}$$

provided that $x \gg 1$.

Apparently, for large arguments, the function quickly converges to zero. In this work, the capillary interaction between spheres is considered to be an approximation of the interaction between cylindrical particles, if the linear size is the length of the particle.

Short-Range Colloid Forces. When two particles get into contact or their surfaces are close (some nms) to each other, the short-range colloid interaction becomes significant.[49,50] The total colloid pair interaction energy can be written in the following form:

$$V_T = V_A + V_R + V_S + V_D \tag{9}$$

where V_A is the van der Waals attraction, V_R is the electric double-layer repulsion, and V_S is the structural interaction energies,[51] which can be either an attractive (hydrophobic) or repulsive (solvation) interaction energy depending on the hydrophobic−hydrophilic nature of the particles' surface. V_D is the dipole−dipole repulsion energy,[52−53] which was introduced as a consequence of an asymmetrical electric double layer around the floating particles at water−fluid interface. Observations show that even though the particles are irreversibly joined together they can change their in-cluster position to an extent determined by the strength and nature of the colloid forces. This process is called restructuring. Strong colloid attraction (e.g., hydrophobic particles on water) can block the restructuring initiated by the long-range capillary forces (the particles are in direct contact). Between particles of high wettability, a thin liquid film of some nms remains, which prevents the assertion of attractive colloid forces; thus, extensive restructuring is allowed.

IV. Experiments

Computer Experiments. The computer simulations were run using the long-range capillary p−p force of the real model presented in section III. In the calculations of forces, an average sphere diameter of 87.5 μm was used and considered to be equivalent to the average cylinder size. The sphere-equivalent diameter (d) of cylinders was approximated by the following relationship: $d = (q + w)/2$, where q and w are the average length and thickness of particles used in real experiments. The effective range of long-range forces was proportional to the length of cylinders in the simulations.

In the simulations, the number of particles was 10 000, the thickness of the particles was 1 pixel, and the particle concentration expressed in surface percent (ratio of the area covered by particles and the reaction plane) was only 3% in order to avoid any disturbing, e.g. gelation, process. Tests were run using 3−4 different values for each of the relevant parameters (effective range of the long-range forces, the extent of restructuring, and the intensity of the surface streams and the anisometry) until the number of clusters reached 50. The actual values of the above parameters were set in the following way:

(i) The effective range of the long-range force, λ^{-1}, was changed using a multiplicative coefficient (a) on the original range:

$$\frac{1}{\lambda_k} = a\frac{1}{\lambda} \tag{10}$$

Greater a commands the longer range. In the simulated experiments, four different values of the multiplicative factor were used to reveal its effect on the aggregation: $a \in \{1.5; 1.2; 1.0; 0.8\}$.

Cluster−Cluster Interaction. the long-range force was computed between every particle pair, which were not in the same cluster. These forces were superposed for each cluster to determine the resulting long-range forces [F(cluster−clusters)] used in the equations of motion. The cluster size is taken into consideration in calculating the cluster motion the following way: (F(cluster−clusters) − $c\bar{v}$)/n, which is proportional to the acceleration of the selected cluster (n is the number of particles belonging to the selected cluster).

The default value of a in the simulations is 1.

(ii) Short-range p−p forces were considered by changing the extent of restructuring. The weaker this force is, the greater the restructuring becomes. We have examined the non-, the weakly, and the strongly restructuring systems and also the effect of particle alignment. Different extents of restructuring and particle alignment were achieved by varying the parameters (Ω_1,Ω_2,Ω_3) of the algorithms that signify the extent of the rotation of clusters (Ω_1), the rotation of particles belonging to a cluster (Ω_2), and the rotation of the freely moving particles (Ω_3). The value of Ω is the Ωth part of the maximum (possible) rotation angle. The maximum angle is 90° for the particle alignment. The examined systems are determined by these triplets: nonrestructuring (0,0,0), weakly restructuring (8,10,20), and strongly restructuring (3,1,1).

The default values for (Ω_1,Ω_2,Ω_3) in the simulations are (0,0,0).

(iii) The effects of the surface flows were investigated by varying four parameters (Y_1,Y_2,Y_3,Y_4). The first parameter in

the quartette set is the number of vortices (both spins are included and their ratio is generated randomly), the second is the number of sources and drains together (their number ratio is generated randomly), the third is the strength of the vortices, and the fourth − the strength of the sources and drains. Higher parameter values cause greater acceleration among the clusters.

We have examined three different systems: one with no flows (0,0,0,0), one with moderate flows (60,60,5000,5000), and one with strong flows (60,60,10 000,10 000) on the surface.

The default parameter setting in the simulations is (30,30,-1000,1000).

(iv) The role of the particles' anisometry was investigated by examining systems of various particle lengths: $q \in \{5; 10; 15; 20$ pixels$\}$.

The default value of q in the simulations is 10.

To verify the validity of the computer model, we have studied the aggregation of polydisperse, rodlike particles at water−air and aqueous surfactant solution−air interfaces, and compared the results to those of the simulation.

Real Experiments. The experimental materials and methods are given below.

Materials. For the aggregation experiments, distilled water, Triton X-100 a nonionic surfactant (concentration, 2 g/100 mL; surface tension measured by Wilhelmy-plate method, 36.8 mN/m; 23 ± 1 °C), and rodlike cylindrical-shaped carbon particles (donation of the University of Ulm, Department of Experimental Physics) of uniform thickness (35 μm) and of polydisperse length (50−350 μm) were used. The density of carbon particles was found to be 1240 kg/m^3.[54] The wettability of carbon rods against water was assessed to be 89° by investigating their floatability at an aqueous alcohol solution−air interface. This procedure was published elsewhere.[54] The wettability of particles against the Triton X-100 solution was assessed by measuring the contact angle (of surfactant solution) using silylated glass plates of about 90° water contact angle. The wetting angle for the surfactant solution was found to be 38°.

Methods. The interfacial aggregation took place in a petri dish. A certain amount of carbon particles was sprinkled on a sieve, and by careful tapping of the frame, it was distributed uniformly on a circular (90 mm diameter) target area of the liquid−air interface. The surface covered by the particles was relatively high, about 8−10% of the total "reaction" area, to reach a reasonable aggregation time. Because of the capillary attraction and the interfacial flows, the particles began to aggregate. The aggregation phenomenon was recorded by a flat bed scanner. The top of the scanner provided the clear white background and a virtually airtight seal of the dish for preventing the external contamination of the model system and for creating a vapor−liquid equilibrium. A snapshot of the aggregation was taken every 5 min, with each pass completed in 70 ± 5 s. This scanning time is a good compromise, because it is short enough that the pattern does not visibly change during one pass and the mechanic parts of the scanner move slow enough not to cause ripples on the surface of the liquid. The images were time-stamped and enhanced by a computer program. By subtracting the prerecorded background (of the liquid filled petri dish, without the carbon particles) from every new image and converting the result to 1-bit binaries, the final data for computer analysis have been obtained.

V. Analysis of Aggregation

The (real and simulated) aggregation was examined from a structural, a kinetic, and a mechanism related property, polydispersity of forming clusters, viewpoint.

Structural Analysis. The structure of the aggregates was analyzed when there were 200 observable clusters. The geometry of the aggregates was characterized by the fractal dimension (D_f) calculated as the rise of the cluster density vs cluster sizes functions[54] for all clusters at this stage. The cluster density (Ψ) was used to characterize the morphology, too. Ψ[47,54] is given by the ratio of the area covered by the particles of the cluster to the total area confined by the boundary layer of the cluster. The higher the Ψ, the denser the structure of cluster investigated.

Kinetic Analysis. The kinetic order of aggregation was investigated by determining the number of clusters as a function of time. If the aggregation is second order, the aggregation rate can be given as follows:[55]

$$-\frac{dn}{dt} = kn^2 \tag{11}$$

where n is the number of clusters in a unit area at time t and k is the rate constant. Integrating the equation with $n(t = 0) = n_0$ results in

$$\frac{1}{n} - \frac{1}{n_0} = kt \tag{12}$$

where n_0 is the initial number of kinetic units/area. Plotting the reciprocal cluster number ($1/n$) as a function of time (t), the rate constant (k) can be calculated from the slope of this curve. The rate constant is proportional to the driving force of the aggregation.

Analysis of Cluster Sizes: Mechanism. The dynamic cluster size distribution functions $n_s(t)$ provide information about the aggregation mechanism. Determining $n_s(t)$, the number of clusters composed of s particles at a time t, we can derive the polydispersity of the forming clusters at a time

$$\pi(t) = \frac{S_M(t)}{S_N(t)} \tag{13}$$

where S_M and S_N are the weight and the number average cluster sizes which can be calculated from the $n_s(t)$ values:

$$S_N(t) = \frac{\sum_s n_s(t)s}{\sum_s n_s(t)} \tag{14}$$

$$S_M(t) = \frac{\sum_s n_s(t)s^2}{\sum_s n_s(t)s} \tag{15}$$

The higher the polydispersity, the broader the cluster size distribution.

In the analysis of the polydispersity of the forming clusters, we have examined how different parameters affect the time evolution of this function. Because in different systems different amounts of time are needed for the aggregation, values of a parameter at a given time are hard to compare. To get around the problem, we defined a kind of "self time"[56] as the reciprocal cluster number ($1/n$). This allows for the comparison of data of states of the same cluster number, independent of the real elapsed time (the number of simulation steps).

In the following section, the results of the model's analysis are presented, along with the effects of reaction parameters on

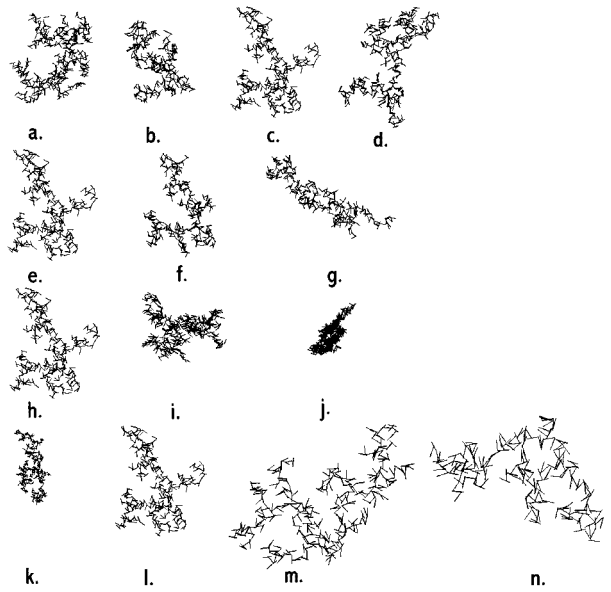

Figure 2. Typical clusters of the examined systems at the same stage of aggregation ($n \approx 200$). The number of particles in the shown clusters is approximately 250−300. The range of the long-range forces where $a = 2.0$ (a), 1.5 (b), 1.0 (c), and 0.8 (d). The strength of the surface streams at (0,0,0,0) (e), (60,60,5000,5000) (f), and (60,60,10 000,10 000) (g). The effect of the short-range forces through the extent of restructuring (Ω_1,Ω_2,Ω_3) (0,0,0) (h), (8,10,20) (i), and (3,1,1) (j). The effect of particle anisometry $q = 5$ (k), 10 (l), 15 (m), 20 (n).

TABLE 1: Structure Parameters of the Studied Systems with D_f Being the Fractal Dimension and Ψ Being the Density of the Clusters

model property	extent	D_f	Ψ
long-range forces	$a = 2.0$	1.77 ± 0.02	0.20 ± 0.03
	$a = 1.5$	1.72 ± 0.02	0.21 ± 0.03
	$a = 1.0$	1.69 ± 0.02	0.22 ± 0.02
	$a = 0.8$	1.66 ± 0.02	0.22 ± 0.04
short-range forces (restructuring parameters)	(0,0,0)	1.69 ± 0.02	0.22 ± 0.03
	(8,5,10)	1.81 ± 0.02	0.29 ± 0.03
	(3,1,1)	1.95 ± 0.02	0.59 ± 0.05
surface streams	(0,0,0,0)	1.67 ± 0.02	0.22 ± 0.05
	(60,60,5000,5000)	1.71 ± 0.02	0.24 ± 0.04
	(60,60,10 000,10 000)	1.76 ± 0.02	0.23 ± 0.03
particle anisometry	20	1.85 ± 0.02	0.10 ± 0.03
	15	1.75 ± 0.02	0.12 ± 0.03
	10	1.69 ± 0.02	0.14 ± 0.04
	5	1.62 ± 0.02	0.40 ± 0.03

the aggregation's structural (D_f and Ψ), kinetic ($1/n$ vs t), and mechanism related (π vs $1/n$ and S_M vs $1/n$) properties (A−E subsections). Then, the model will be tested comparing the results to those of real experiments (F subsection).

VI. Results and Discussion

Simulation Results for the Long-Range p−p Interaction. Typical clusters of the examined systems are shown in Figure 2a−d, and the corresponding structure parameters are presented in the appropriate lines of Table 1. Increasing the effective range of the attractive force shows as a significant increase in D_f. It is interesting to note that the cluster density (Ψ) is insensitive to this change. The relatively high values of D_f (without restructuring) and their rising tendency (from 1.66 up to 1.77) indicate that the aggregation becomes increasingly percolation-like with increasing effective range of the attraction force. For comparison, the theoretical value of the fractal dimension for a percolation cluster is 1.89,[57] and for the diffusion-limited cluster−cluster aggregation, 1.44.[58] It means that our system is in a transition range concerning the chosen surface concentration, anisometry, and the effective range of the driving force of aggregation.

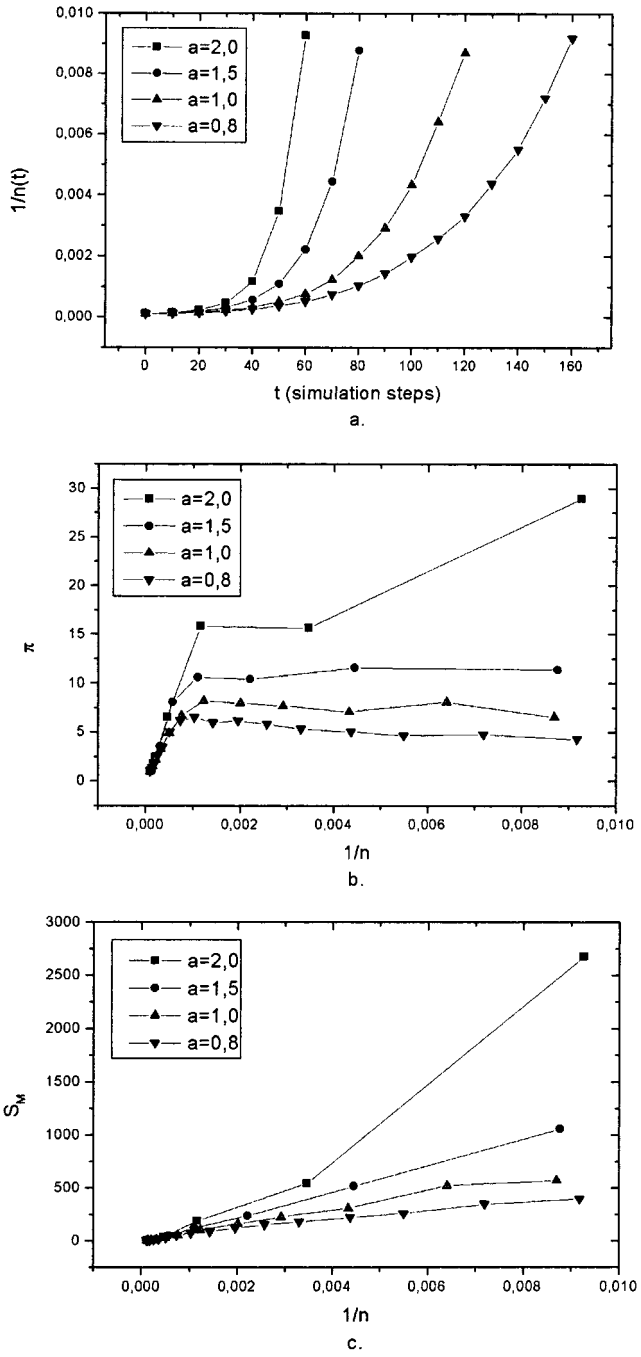

Figure 3. Effects of long-range forces on the aggregation. (a) $1/n$ vs t, (b) π vs $1/n$, and (c) S_M vs $1/n$, where n is the number of clusters, S_M is the weight average cluster size, π is the polydispersity, and a is the range correction factor.

The effect of the change in the effective range of the attractive force on the aggregation kinetics is shown in Figure 3a. The rate constants (derived from the initial, nearly linear, part of the kinetic curves) can be seen in Table 2. As can be seen, the increasing effective range of the forces causes a significant rise in the value of the kinetic constants, giving the curves an increasing rise. This shows that the driving force of the aggregation is greater. As the aggregation progresses, greater clusters appear, and their increasing hydrodynamic resistance cannot compensate for the influence of the increasing capillary

TABLE 2: Kinetic Constants (k) of the Studied Systems which Are the Derivates of the First Linear Interval of the Curves[a]

model property	extent	k
long-range forces	$a = 2.0$	11.5 ± 3.4
	$a = 1.5$	6.6 ± 1.7
	$a = 1.0$	3.6 ± 0.9
	$a = 0.8$	2.6 ± 0.5
short-range forces (restructuring parameters)	(0,0,0)	7.6 ± 1.5
	(8,5,10)	7.0 ± 1.3
	(3,1,1)	6.9 ± 1.2
surface streams	(0,0,0,0)	7.4 ± 1.4
	(60,60,5000,5000)	8.7 ± 1.8
	(60,60,10 000,10 000)	9.1 ± 1.9
particle anisometry	20	10.0 ± 2.3
	15	8.7 ± 1.9
	10	7.6 ± 1.5
	5	6.0 ± 1.0

[a] k is expressed in arbitrary units.

forces; again, the driving force of the aggregation increases. This observation corresponds well to previous results for simulations with spherical particles.[47]

The dependence of the polydispersity of the forming clusters on the effective range is shown in Figure 3b; decreasing effective range results in decreasing polydispersity. In line with the above observation for cylindrical particles, the weight average size of clusters shows a decrease as the effective range of the long-range forces decrease (Figure 3c). It is interesting to note that earlier a reverse dependence was observed for spherical particles at the same surface concentration.[47] It also shows that because of the high particle anisometry a percolation-like aggregation takes place in this present case, manifesting itself in an unexpected dependence of polydispersity functions on the driving force of aggregation.

Simulation Results for the Short-Range p−p Interaction (Restructuring). Representative clusters of the examined systems are shown in Figure 2h−j, and their structure parameters are shown in Table 1. After examining the effects of the restructuring on the structure, it is clear that more intense restructuring causes greater D_f and greater Ψ. Because of restructuring, the particles of the clusters get closer to each other, and the clusters become denser and more compact; thus, the increasing D_f and Ψ is easily interpreted.

Kinetic curves of the examined systems are shown in Figure 4a; the kinetic constants derived from the beginning nearly linear part of the kinetic curves are presented in Table 2. In Figure 4a, it is quite apparent that in the early stages of the aggregation the kinetic curves run with a uniform rise; thus, no significant change can be found among the kinetic constants. However, in the second stage of the aggregation, the kinetic curves acquire a different rise; this shows that the driving force of the aggregation is smaller if the extent of the restructuring is greater. The reason for this is supposedly that restructured clusters, of a large number of particles, occupy less surface area, because of their high compactness and density; therefore, the probability of their collision is also smaller.

In a later stage of the aggregation, the polydispersity gets lower if the restructuring intensifies (Figure 4b) which is in a good agreement to the above statement about the correlation of driving force and polydispersity. This result also correlates well with the observation that more intense restructuring causes a decrease in the weight average of cluster sizes at a given self-time of aggregation (see Figure 4c).

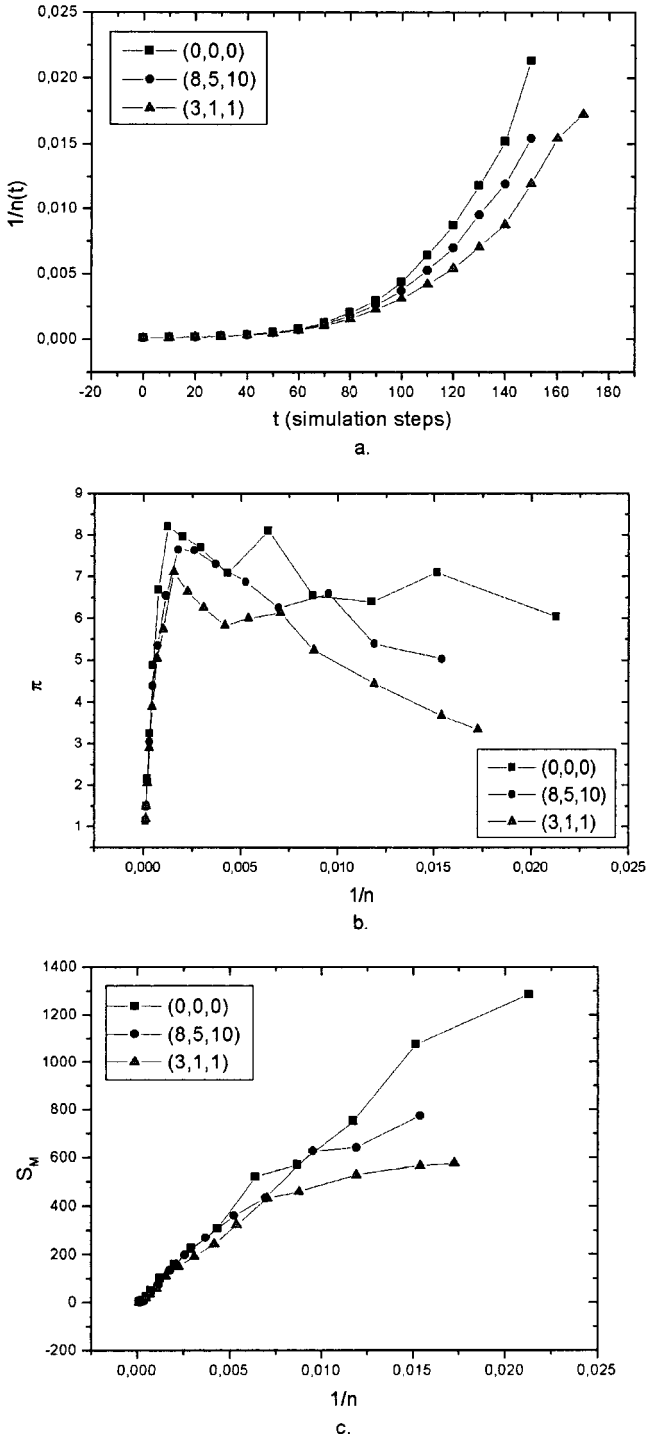

Figure 4. Effects of short-range forces on the aggregation. (a) $1/n$ vs t, (b) π vs $1/n$, and (c) S_M vs $1/n$, where n is the number of clusters, S_M is the weight average cluster size, π is the polydispersity, and the numbers in the parentheses are the values of (Ω_1,Ω_2,Ω_3).

Simulation Results for the "Surface Streams". As it can be seen in Figure 2e−g and Table 1, increasing the intensity of "surface-flows" results in a subtle rise in D_f and no significant change in Ψ in the observed interval. This effect cannot be interpreted yet.

The effects of the "surface flows" on the aggregation kinetics are shown in Figure 5a and in Table 2. It is clear from Figure 5a that increasing flows only cause significant changes in the steepness of the kinetic curves in the middle of the aggregation. Increasing flows result in a steeper curve revealing an increasing driving force of aggregation at this stage. The reason for this

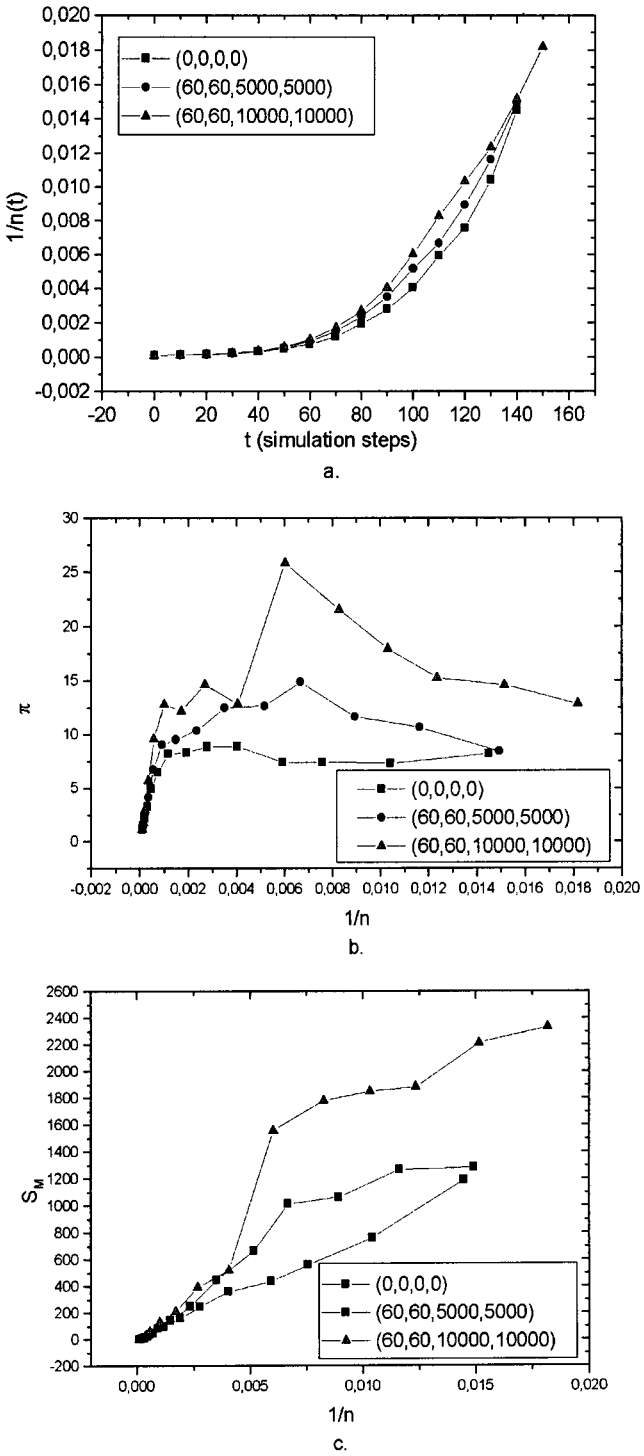

Figure 5. Effects of the surface flows on the aggregation. (a) $1/n$ vs t, (b) π vs $1/n$, and (c) S_M vs $1/n$, where n is the number of clusters, S_M is the weight average cluster size, π is the polydispersity, and the numbers in the brackets are in order of appearance: the number of vortices and sources/drains and their intensity.

behavior cannot be understood yet. Perhaps, there are some correlations between the flow parameters and the characteristic linear sizes of forming clusters and/or the cluster−cluster distances.

Because of the increasing intensity of the flows, the polydispersity and the average cluster-size shows an incrementing tendency (see Figure 5b,c), also demonstrating an increasing driving force with the increasing flow intensities. The most important result for the "surface streams" is that an increase in the flow intensity leads to an increase in the driving force of aggregation.

Simulation Results on Particle Anisometry. The effects of the particle anisometry have been tested using four distinct particle-lengths: $q \in \{5; 10; 15; 20$ pixels$\}$. From Table 1, it is apparent that the increasing anisometry of the particles commands a decreasing tendency in the values of Ψ as required. On the contrary, D_f shows a significant increase with increasing particle anisometry, which is also reasonable, considering that increasing particle anisometry corresponds to increasing particle size. On the one hand, the increasing particle size results in an increase in the effective range of the long-range forces, which, as was shown in a previous section of this paper, leads to higher fractal dimensions. On the other hand, the increasing anisometry of particles can result in lowering the concentration threshold of percolation, leading to higher fractal dimensions.

Increasing particle anisometry causes the kinetic constant to increase. According to Figure 6a, the positive deviation of the curves is accentuated by the increasing anisometry of the particles. The reason for this could very well be that particles of greater anisometry form larger clusters of lower density that have a greater chance to collide with others, resulting in a greater driving force for the aggregation. On the other hand, with increasing anisometry, the effective range of the attractive forces will also increase, manifesting itself in an increasing driving force of the aggregation.

Increasing particle anisometry commands a rising tendency in the polydispersity (see Figure 6b). This observation confirms the conclusions above about the relation of driving force and polydispersity. Increasing particle anisometry corresponds to greater driving force, which results in higher polydispersity in the investigated systems. This explanation is also supported by Figure 6c, which shows that greater anisometry causes the value of S_M to rise at the same self-time.

Comparison of the Results of Simulations and Real Experiments. We have studied the aggregation of polydisperse ($\pi = 1.2$) rodlike carbon particles at water−air and aqueous surfactant solution−air interfaces and compared the results of real and computer experiments. The surface covered by the particles was 8% of the total "reaction" area in the computer simulations in the present simulations. The long-range forces were calculated by eq 3 applying the characterizing parameters of real systems (surface tension, contact angle, and particle density). Because of the new parameter setting, the greatness of the attractive, long-range forces was significantly diminished. When the nonrestructuring system, for example, was simulated, the forces only reached the 25% of those of simulations for the previous analysis (Figures 1−6). The long-range (capillary) forces as a function of particle−particle distances, calculated by the computer model, for water−air and surfactant solution−air interfaces are given in Figure 7. As it can be seen, the capillary attraction is stronger for the water−air interface. For comparison, the effective range of the long-range forces at the default particle length of 10 pixels is 310 and 220 pixels for the water and for the surfactant solution subphases, respectively.

We show characteristic images of clusters formed in real (Figure 8a,b) and in computer experiments (Figure 8c,d), for nonrestructuring (Figure 8a,c) and for restructuring (Figure 8b−d) systems. The similarity of the corresponding images is obvious. The corresponding cluster density values (Ψ) in Table 3 also confirm the visual observations. The fractal dimensions of real and simulated systems are also similar to one another. Their relatively lower values do not show percolation-like mechanism due to the weaker particle−particle attraction.

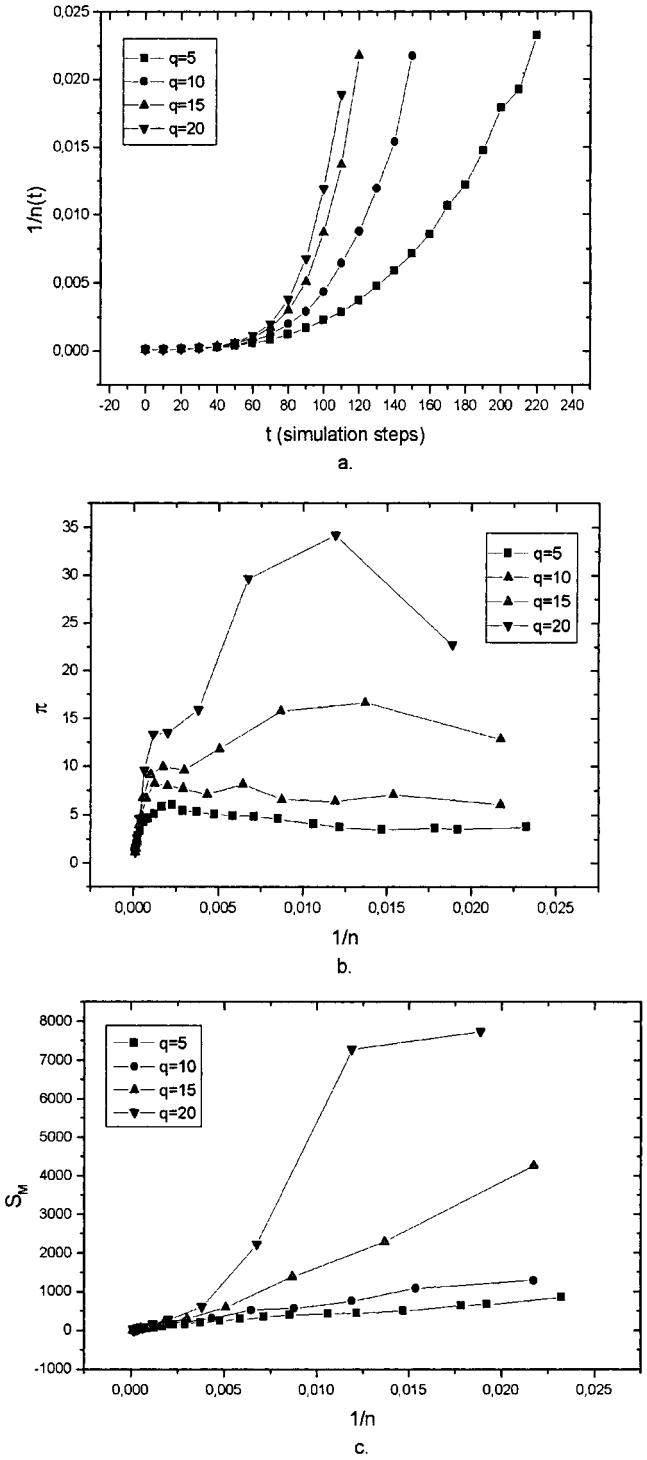

Figure 6. Effects of particle-anisometry on the aggregation. (a) $1/n$ vs t, (b) π vs $1/n$, and (c.) S_M vs $1/n$, where n is the number of clusters, S_M is the weight average cluster size, π is the polydispersity, and q is the length of the paricles in pixels.

The $1/n$ vs t curves of the polydisperse rodlike carbon particles aggregating at water−air and aqueous surfactant solution−air interfaces are presented in Figure 9a,b for real and in Figure 10a,b for computer experiments. Comparison of the results brings us to conclude that the aggregation requires more time at aqueous surfactant solution−air than at water−air interfaces, both in simulation and in real experiments. The kinetic curves have two sections; first, they run with a small rise, then at a specific time, the rise increases. The (k_1, k_2) kinetic constants that are the characteristic rises of the sections are

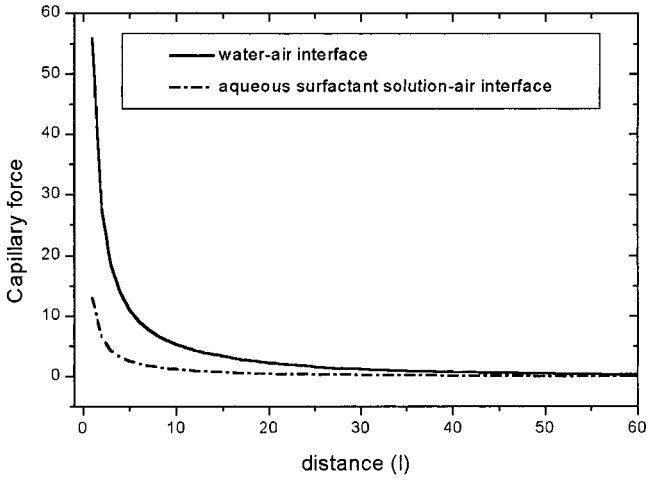

Figure 7. Long-range (capillary) forces as a function of particle−particle distances (l) calculated by the computer model for water−air and aqueous surfactant solution−air interfaces. Both parameters are given in pixels.

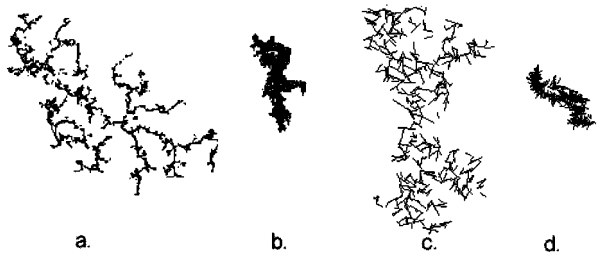

Figure 8. Characteristic clusters of aggregating polydisperse, rodlike particles at water−air and aqueous surfactant solution−air interfaces in real (a and b) and computer (c and d) experiments. The clusters were selected at the same self-time of aggregation ($1/n = 1/200$). The images are pixelated due to the high magnification.

TABLE 3: Structure Parameters of the Observed Systems (Figure 8) with D_f Being the Fractal Dimension and Ψ Being the Cluster Density

experiment	system	D_f	Ψ
real	nonrestructuring	1.43 ± 0.02	0.24 ± 0.03
	restructuring	1.75 ± 0.04	0.88 ± 0.02
simulation	nonrestructuring	1.47 ± 0.06	0.20 ± 0.03
	restructuring	1.78 ± 0.06	0.84 ± 0.04

shown in Table 4. It can easily be seen that the kinetic constants for a given section are lower at aqueous surfactant solution−air interfaces. To compare the real and the computer experiments, we have taken the ratio of the kinetic constants of restructuring (aqueous surfactant solution-air interface) and nonrestructuring (water−air interface) systems for both sections. The ratios in Table 5 show a strong correlation between the simulations and the real experiments, supporting the faithfulness of the aggregation model.

The π vs $1/n$ curves of carbon particles aggregating at aqueous surfactant solution−air interfaces are shown in Figures 9c and 10c for real and computer experiments. From the graphs, it is apparent that, at a given number of clusters, polydispersity is greater at water−air interfaces both in real and in computer experiments. Higher polydispersity means that the size distribution of the clusters is more polarized: only a few great clusters form collecting individual particles and smaller clusters (the size distribution interval is wider).

This result is contrary to the results of the previously studied aggregating glass beads.[47] Their polydispersity for the hydrophilic (restructuring) systems was greater than that of hydro-

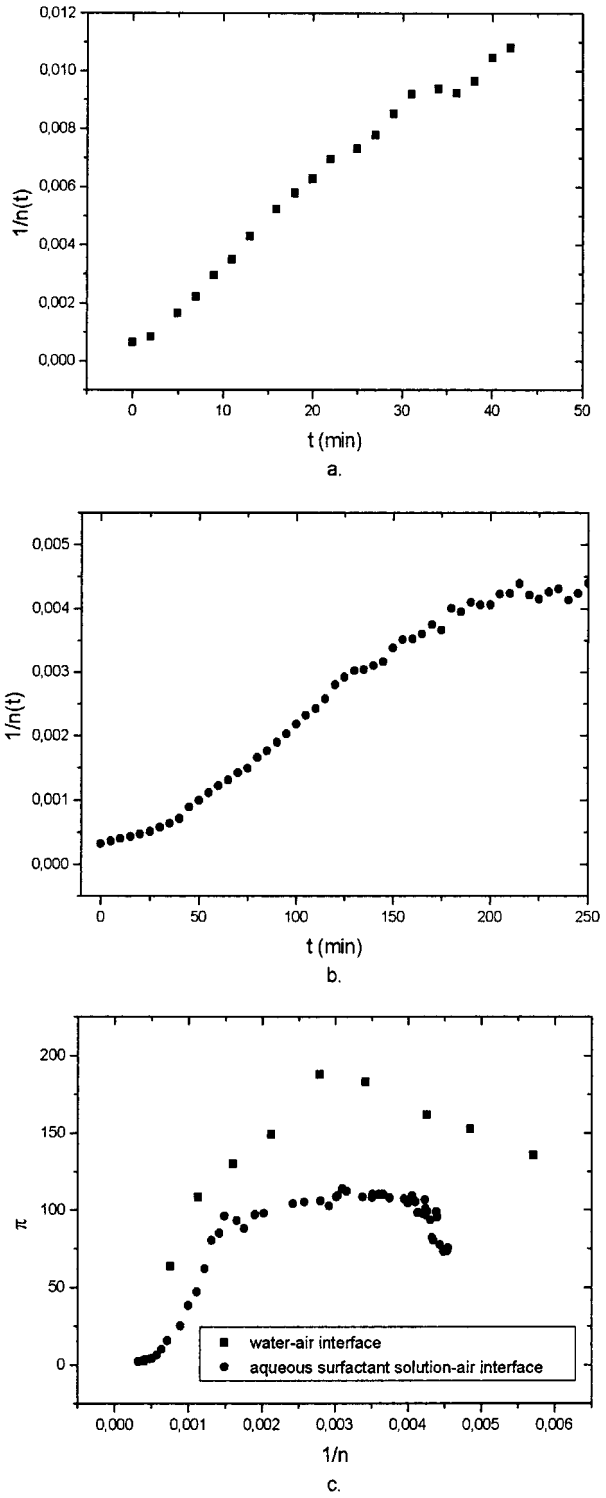

Figure 9. Kinetic curves of polydisperse, rodlike carbon particles at (a) water−air and at (b) aqueous surfactant solution−air interfaces, and (c) the π vs $1/n$ curves for both interfaces.

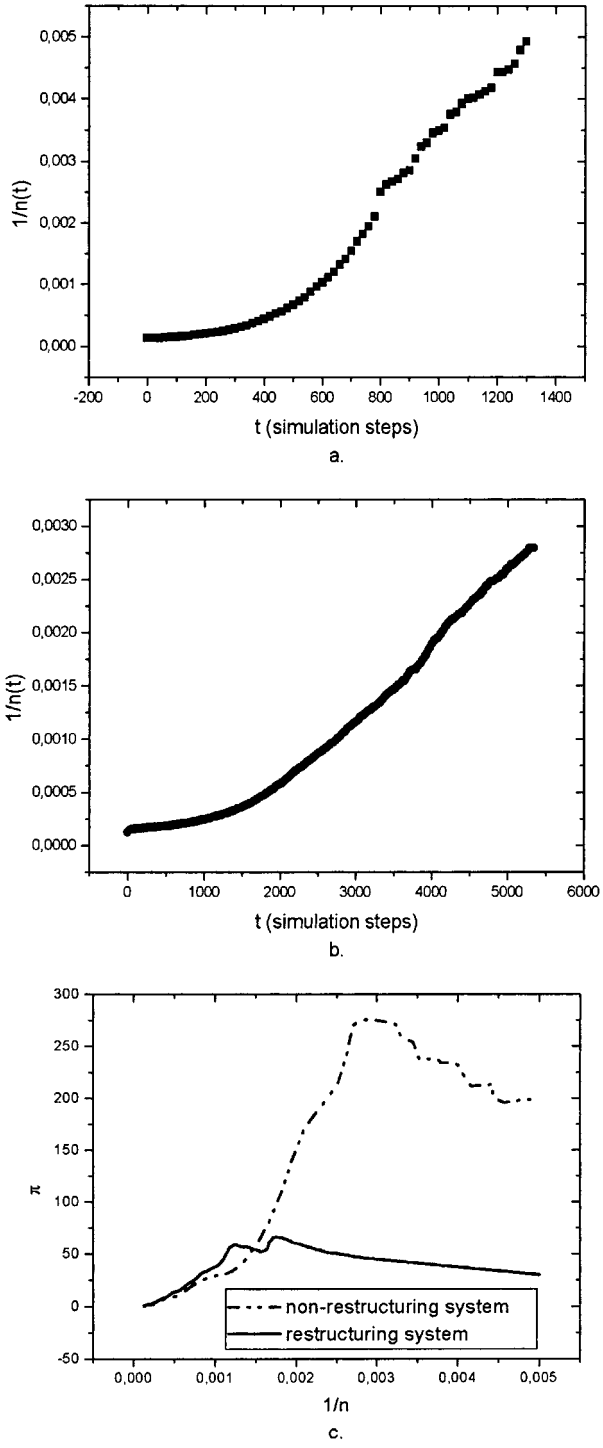

Figure 10. Kinetic curves of aggregating polydisperse, rodlike carbon particles for (a) "nonrestructuring" and for (b) "restructuring" systems, and (c) the π vs $1/n$ curves for both systems (t is given in simulation steps).

phobic, nonrestructuring systems. Our explanation, again, is that the cause of this difference is that the gel point (i.e., percolation threshold)[58−60] is lower for rods than for spheres and the growth mechanism in the system of rodlike carbon particles differs from that of the aggregating spheres, also compared to the correlation between the fractal dimensions and the particle lengths in Table 1. Interestingly, the different mechanism does not manifest itself in the fractal dimensions in the real conditions. It should be noted that by decreasing the concentration of the rods in the simulation (to 2%), we get the same results for the clusters' polydyspersity as for spherical particles (see Figure 11).

Conclusion

An off-lattice computer model for the 2D aggregation of anisometric (cylindrical-shaped) particles, mainly based on molecular dynamics, was developed and tested by investigating the interfacial aggregation of cylindrical-shaped carbon microparticles at liquid−air interfaces.

TABLE 4: Kinetic Constants (k_1,k_2,k_3,k_4) of Interfacial Aggregations of Polydisperse, Rodlike Carbon Particles in Real and Computer Experiments[a]

	kinetic constants			
	real		simulation	
system	k_1	k_2	k_3	k_4
nonrestructuring	9.7×10^{-5}	28.3×10^{-5}	11.3×10^{-5}	60.4×10^{-5}
restructuring	0.9×10^{-5}	2.6×10^{-5}	1.0×10^{-5}	5.8×10^{-5}

[a] The value of k is given in cm^2/s in the real experiments and in arbitrary units in the simulations.

TABLE 5: Ratios of the Kinetic Constants in Real and in Computer Experiments for the Different Sections (1 and 2) of the Kinetic Functions[a]

	ratios of the kinetic constants	
experiments	section 1: k(n-rest.)/k(rest.)	section 2: k(n-rest.)/k(rest.)
real	11.2	11.1
simulation	11.2	10.5

[a] k(n-rest.) and k(rest.) are the kinetic constants for the nonrestructuring and for the restructuring systems.

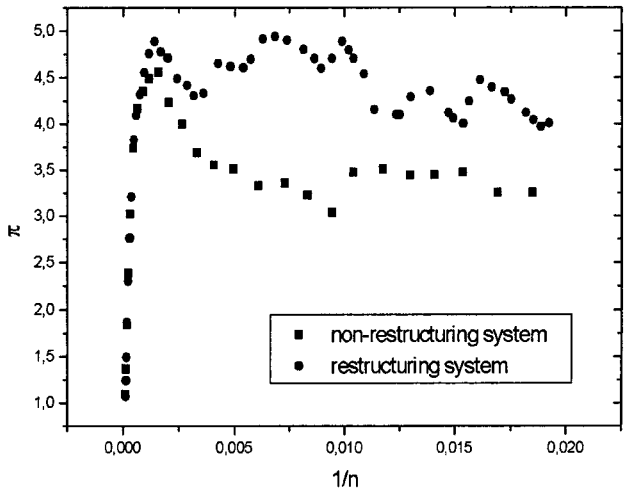

Figure 11. π vs $1/n$ curves of rodlike particles at 2% surface concentration, in "nonrestructuring" and in "restructuring" systems from computer simulations.

According to the computer simulations, the increasing driving force of aggregation always resulted in the increase of fractal dimensions even if no restructuring was allowed. The polydispersities of the forming clusters as a function of self-time of aggregation also showed an increase with the increasing driving force.

On the contrary, the real systems always showed restructuring depending on the particle wettabilities. Significant restructuring occurred at lower contact angles (at aqueous surfactant solution−air interfaces), resulting, as expected, in higher fractal dimensions than that of the samples with higher contact angles (at water−air interfaces), though the driving force of aggregation was weaker. The stronger driving force, however, also led to higher polydispersities for the real systems.

The analysis of the results in comparison with a previous finding[47] led to the conclusion that the aggregation of rodlike particles under the present conditions shows a transition between a diffusion-limited-like aggregation and percolation.

Acknowledgment. Support for this work in the form of grants from OTKA (T030457 to Z.H. and T015754 to M.Z.) and from NSERC (to M.N.E.) is gratefully acknowledged.

References and Notes

(1) Martin, J. E.; Wilcoxon, J. P.; Schaefer, D.; Odinek, J. *Phys. Rev. A* **1990**, *41*, 4379.
(2) Earnshaw, J. C.; Harrison, M. B.; Robinson, D. *J. Phys. Rev. E* **1996**, *53*, 6155.
(3) Earnshaw, J. C.; Robinson, D. *J. Physica A* **1995**, *214*, 23.
(4) Earnshaw, J. C.; Robinson, D. *J. Phys. Rev. Lett.* **1994**, *72*, 3682.
(5) Robinson, D. J.; Earnshaw, J. C. *Phys. Rev. Lett.* **1993**, *71*, 715.
(6) Hidalgo-Álvarez, R.; Martin, A.; Fernandez, A.; Bastos, D.; Martinez, F.; de las Nieves, F. J. *Adv. Colloid Interface Sci.* **1996**, *67*, 1.
(7) Fernandez-Barbero, A.; Schmitt, A.; Cabrerizo-Vilchez, M.; Martinez-Garcia, R. *Physica A* **1996**, *230*, 53.
(8) Earnshaw, J. C.; Robinson, D. J. *J. Phys. Condens. Mater.* **1995**, *7*, 397.
(9) Meakin, P. *Adv. Colloid Interface Sci.* **1988**, *28*, 249.
(10) Dodson, C. T. *J. Tappi J.* **1996**, *79*, 211.
(11) Bousfield, D. W. *Nordic Pulp Paper Res. J.* **1993**, *8*, 176.
(12) Kerekes, R. J.; Schell, C. *J. Tappi J.* **1995**, *78*, 133.
(13) Németh, Zs.; Halász, L.; Pálinkás, J.; Bóta, A.; Horányi, T. *Colloids Surf., A* **1998**, *145*, 107.
(14) Németh, Zs.; Halász, L.; Pálinkás, J.; Bóta, A.; Horányi, T. *Tenside Surf. Deter.* **1999**, *36*, 88.
(15) Ganesan, V.; Fredrickson, G. H. *J. Rheology* **2001**, *45*, 161.
(16) Yamane, Y.; Kaneda, Y.; Doi, M. J. *Non-Newtonian Fluid Mech.* **1994**, *54*, 405.
(17) Yamamoto, S.; Matsuoka, T. *J. Chem. Phys.* **1993**, *98*, 644.
(18) Yamamoto, S.; Matsuoka, T. *J. Chem. Phys.* **1995**, *102*, 2254.
(19) Yamamoto, S.; Matsuoka, T. *Polym. Eng. Sci.* **1995**, *35*, 1022.
(20) Skjetne, P.; Ross, R. F.; Klingenberg, D. J. *J. Chem. Phys.* **1997**, *107*, 2108.
(21) Ross, R. F.; Klingenberg, D. J. *J. Chem. Phys.* **1997**, *106*, 2949.
(22) Ross, R. F.; Klingenberg, D. J. *J. Pulp Paper Sci.* **1998**, *24*(12), 994.
(23) Allain, C.; Jouhier, B. *J. Phys. (France) Lett.* **1983**, *44*, l.
(24) Hurd, A. J.; Schaefer, D. W. *Phys. Rev. Lett.* **1985**, *54*, 1043.
(25) Skjeltorp, A. T. *Phys. Rev. Lett.* **1987**, *58*, 1444.
(26) Skjeltorp, A. T.; Helgesen, G. *NATO ASI Ser. E* **1988**, *157*, 56.
(27) Roussel, J.-F.; Camoin, C.; Blanc, R. *J. Phys. (Paris)* **1989**, *50*, 3259.
(28) Roussel, J.-F.; Camoin, C.; Blanc, R. *J. Phys. (Paris)* **1989**, *50*, 3269.
(29) Robinson, D. J.; Earnshaw, J. C. *Phys. Rev. A* **1992**, *46*, 2045.
(30) Robinson, D. J.; Earnshaw, J. C. *Phys. Rev. A* **1992**, *46*, 2055.
(31) Robinson, D. J.; Earnshaw, J. C. *Phys. Rev. A* **1992**, *46*, 2065.
(32) Williams, D. F.; Berg, J. C. *J. Colloid Interface Sci.* **1992**, *152*, 218.
(33) Kralchevsky, P. A.; Nagayama, K. *Langmuir* **1994**, *10*, 23.
(34) Robinson, D. J.; Earnshaw, J. C. *Langmuir* **1993**, *9*, 1436.
(35) Onoda, G. Y. *Phys. Rev. Lett.* **1985**, *55*, 2263.
(36) Armstrong, A. J.; Mockler, R. C.; O'Sullivan, W. J. *J. Phys.: Condens. Matter* **1989**, *1*, 1707.
(37) Levine, S.; Bowen, B. D. *Colloids Surf. A* **1993**, *70*, 33.
(38) Aveyard, R.; Beake, B. D.; Clint, J. H. *J. Chem. Soc., Faraday Trans.* **1996**, *92*, 4271.
(39) Aveyard, R.; Clint, J. H. *J. Chem. Soc., Faraday Trans.* **1995**, *91*, 2681.
(40) Menon, V. B.; Nikolov, A. D.; Wasan, D. T. *J. Colloid Interface Sci.* **1988**, *124*, 317.
(41) Meldrum, F. C.; Kotov, N. A.; Fendler, J. H. *J. Phys. Chem.* **1994**, *98*, 4506.
(42) Kotov, N. A.; Meldrum, F. C.; Wu, C.; Fendler, J. H. *J. Phys. Chem.* **1994**, *98*, 2735.
(43) Tolnai, Gy.; Csempesz, F.; Kabai-Faix, M.; Kálmán, E.; Keresztes, Zs.; Kovács, A. L.; Ramsden, J. J.; Hórvölgyi, Z. *Langmuir* **2001**, *17*(9), 2683.
(44) Aveyard, R.; Binks, B. P.; Fletcher, P. D. I.; Rutherford, C. E. *Colloids Surf., A* **1994**, *83*, 89.
(45) Hadjiiski, A.; Dimova, R.; Denkov, N. D.; Ivanov, I. B.; Borwankar, R. *Langmuir* **1996**, *12*, 6665.
(46) Hórvölgyi, Z.; Németh, S.; Fendler, J. H. *Langmuir* **1996**, *12*, 997.
(47) Vincze, A.; Agod, A.; Kertész, J.; Zrínyi, M.; Hórvölgyi, Z. *J. Chem. Phys.* **2001**, *114*, 520.
(48) Chan, D. Y. C.; Henry, J. D., Jr.; White, L. R. *J. Colloid Interface Sci.* **1981**, *79*, 410.
(49) Hórvölgyi, Z.; Máté, M.; Zrínyi, M. *Colloids Surf., A* **1994**, *84*, 165.
(50) Máté, M.; Zrínyi, M.; Hórvölgyi, Z. *Colloids Surf., A* **1996**, *108*, 147.
(51) Derjaugin, B. V.; Churaev, N. V. *Colloids Surf.,* **1989**, *41*, 223.
(52) Pieranski, P. *Phys. Rev. Lett.* **1980**, *45*, 569.
(53) Martínez-López, F.; Cabrerizo-Vílchez, M. A.; Hidalgo-Álvarez, R. *J. Colloid Interface Sci.* **2000**, *232*, 303.

(54) Vincze, A.; Fata, R.; Zrínyi, M.; Hórvölgyi, Z.; Kertész, J. *J. Chem. Phys.* **1997**, *107*, 7451.
(55) Sonntag, H.; Strenge, K. *Coagulation kinetics and structure formation*; Plenum: New York, 1987.
(56) Agod, A.; Vincze, A.; Kertész, J.; Zrínyi, M.; Hórvölgyi, Z. *Proc. of Vegyészkonferencia*, in Hungarian; *Erdélyi-Magyar Mûszaki Tudományos Társaság*: Kolozsvár, Romania, **2000**, 85.
(57) Gould, H.; Tobochnik, J. *An Introduction to Computer Simulation Methods*; Addison-Wesley: Cambridge, 1988; Vol. 2.
(58) Vicsek, T. *Fractal Growth Phenomena*, 2nd ed.; World Scientific: Singapore, 1992.
(59) Vicsek, T.; Kertész, J. *Phys. Lett.* **1981**, *81A*, 51.
(60) Hórvölgyi, Z.; Fendler, J. H.; Máté, M.; Zrínyi, M. *Prog. Colloid Polym. Sci.* **1996**, *102*, 126.